Progress In Electromagnetics Research M, Vol. 65, 79–90, 2018

Novel Adaptive Buried Nonmetallic Pipe Crack Detection Algorithm for Ground Penetrating Radar

Prabhat Sharma[1], Bambam Kumar[2], and Dharmendra Singh[2, *]

Abstract—Ground penetrating radar (GPR) may be used to detect cracks in a buried pipe. Using GPR, there are only a few techniques, such as statistical approach robust principal component analysis (RPCA). to detect cracks in buried objects. Buried nonmetallic pipe crack detection is an important application for GPR to analyze the structural health of underground pipelines. The strength of a reflected signal may be feeble from a cracked location as compared to position with respect to that from other positions of the pipe. Currently, crack detection is a challenging task, especially when the buried pipe is nonmetallic, and soil moisture varies. In this paper, the problem of crack detection in a PVC pipe using GPR is attempted. It is a challenge to detect small sized cracks in an underground PVC pipe because the GPR image is flooded with correlated background signal or clutter, and the image patterns are typically irregularly distributed. In order to efficiently detect the crack in a buried PVC pipe, a novel adaptive crack detection algorithm has been developed with the help of covariance of real GPR data and covariance of normal distributed synthetic Gaussian data. Results are evaluated and validated to show the effectiveness of crack detection algorithm.

1. INTRODUCTION

A ground-penetrating radar (GPR) images subsurface structures by transmitting short electromagnetic pulses into the ground and receiving reflections [1]. It is considered as one of the most promising technologies for close detection and identification of buried targets, due to its ability of detecting nonmetallic objects in the subsurface. There are a lot of methods proposed by researchers to detect nonmetallic targets with clutter reduction. First, mean removal method subtracts the mean from each total field trace. Only steady background or random noise can be removed by mean removal method [2]. The second method, median removal [2] approach for clutter subtraction, is the same in a broad sense as the mean removal approach [2]. This method is suitable to reduce abrupt internal noise, which usually occurs in a time series signal. High dielectric constant targets can be detected by estimating the signal of interest and noise using singular value decomposition (SVD) for nonlinear surface [3]. Principal component analysis (PCA) [4, 6] is a second order statistical (zero mean) method, which reduces the dimension of data and uses decorrelation property. Primarily, independent component analysis (ICA) [4] is used to solve blind source separation problem. ICA divides GPR data into statistically independent components while another techniques such as PCA represents data as uncorrelated components. Since decorrelation property is not enough to separate signals efficiently, statistical independence is used in ICA. However, both PCA and ICA methods provide good results for metallic targets and for low soil moisture level [5]. Therefore, when GPR is used to detect low dielectric constant objects like PVC pipe, etc., it is difficult to extract the target information in various soil conditions. It is a challenging task to detect cracked and non-cracked PVC pipes. Another aspect is that if a buried PVC pipe is cracked, then

Received 10 October 2017, Accepted 23 January 2018, Scheduled 2 March 2018
* Corresponding author: Dharmendra Singh (dharmendrasing@yahoo.com).
[1] Instruments Research and Development Establishment, Dehradun, Uttarakhand, India. [2] Electronics and Communication Engineering Department, Indian Institute of Technology Roorkee, Roorkee, Uttarakhand, India.

there is a need to detect the crack along with detection of PVC pipe. Researchers have used robust principal component analysis (RPCA) method [14] for crack feature extraction from the correlated background in GPR concrete inspection on synthetic data. Few researchers have used adaptive statistical approach for non-destructive underline crack detection of ceramic tiles using millimeter wave Imaging Radar for industrial application [17]. In this paper, our main objective is to detect a nonmetallic PVC pipe and if it is cracked then to detect the crack position with the help of indigenously developed GPR. Here, we use real data to extract crack features. This paper is organized as follows. Section 2 provides GPR system description and experimental details for detecting the PVC pipe with crack. Section 3 discusses the detail of developed algorithm and implementation for detecting cracked PVC pipe. Section 4 provides results and discussion of the developed technique. Finally, Section 5 summarizes the conclusion of the work.

2. EXPERIMENTAL SETUP FOR CRACK DETECTION

The experimental GPR setup for crack detection is shown in Figure 1. It consists of a double-ridge horn antenna, a transceiver (TX/RX) unit, and a signal processing unit. Overall specifications of the GPR setup [18] and experimental parameters are listed in Table 1(a). More than 500 data have

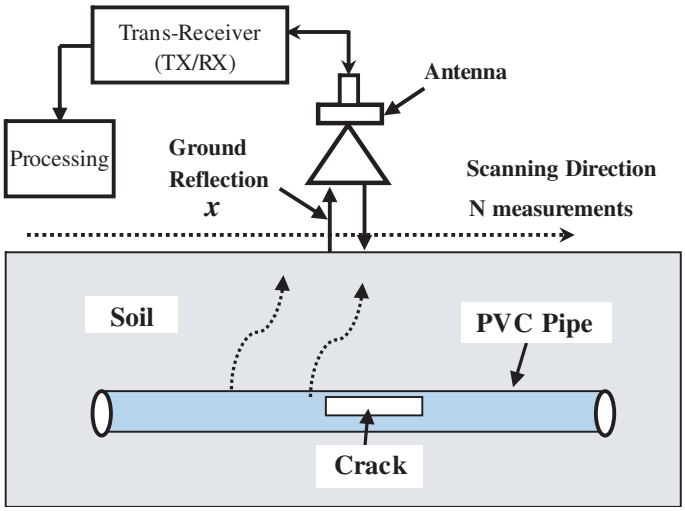

Figure 1. Experimental setup for crack detection.

Table 1. Experimental details with (a) GPR specifications, (b) target description and experimental parameters.

Table 1(a): The Specification of GPR setup.

GPR Active Radar Parameter	Typical Value
Operating frequency	1 GHz–2 GHz
No. of frequency points (M)	631
Transmitted Power	1 mW
Antenna type	Double Ridge Horn Antenna
Range Resolution	15 cm
Antenna Height from ground	15 cm
Investigated Depth	$\leq$ 1 m
No. of cross range points (N)	20
Frequency step size (Δf_0)	1.58 MHz

Table 1(b) Target description and experimental parameters.

Target used for GPR system	Target description
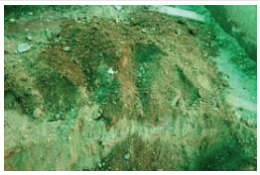	Ground Ground field area for experiment at Indian Institute of Technology, Roorkee with soil moisture variation of 5-15% in 5% intervals,GND_1= 5%,GND_2=10% and GND_3=15% (Results are shown only for GND_3 ground data)
	Target-1 Type: Without Cracked non-metallic Pipe Material: PVC Dimensions : (Length x Diameter =225 cm ×5 cm) Burial depth; 15 cm-50 cm in 5 cm intervals and each depth dataset measured with 5%, 10% and 15% soil moisture, e.g., (Target-1,$Dataset_{13}$) = 35 cm depth and 10 % soil moisture (Results are shown only for Target-1 $Dataset_{21}$, i.e., 30 cm depth and 15% Soil Moisture)
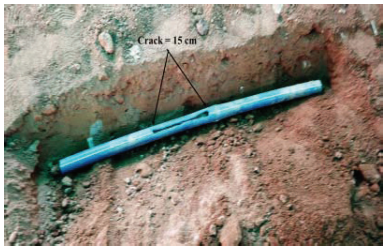	Target-2 Type: Cracked non-metallic Pipe Material: PVC Dimensions : (Length ×Diameter =225 cm ×5 cm) (Results are shown only for target-2 $Dataset_{21}$=30 cm depth, Cracksize = 15 cm and 15% Soil Moisture) 15 cm-50 cm in 5 cm interval and each depth dataset measured with 5%, 10% and 15% of soil moisture, e.g., (Target-1,$Dataset_{13}$) = 35 cm depth and 10 % soil moisture

*In Table 1(b), collected data have been denoted by (targets, Dataset'$_i$).
*Targets may be ground, target-1 (i.e., Without Cracked PVC pipe), target-2 (i.e., Cracked PVC pipe).
*Dataset'$_i$ denotes collected data for the corresponding target, where subscript *i* represents the collected data number for particular depth and moisture.

been collected for analyzing the GPR-based crack detection. In this experiment, a crack size 15 cm is considered because GPR resolution is limited to 15 cm. The soil moisture of field was varied from 5% to 15% in steps of 5% and burial depth of target varied from 15 cm to 50 cm in steps of 5 cm for Target-1 (non-cracked PVC pipe) and Target-2 (cracked PVC pipe). GPR A-scan and B-scan were carried out, details of which are given in [18]. The 1D GPR range profile is called as A-scan and when a number of A-scans are collected in the GPR data processing, which form a 2D matrix of a GPR image of the area of interest, it is known as B-scan.

2.1. Problem Formulation

For detecting the crack in a buried PVC pipe, the problem can be formulated as follows:

(i) Assume that a low dielectric PVC pipe which has a dielectric constant of approximately 3 [19] is buried in the ground with soil moisture content varying from 5% to 15% at depths mentioned in Table 1(b). There is a crack in the PVC pipe at some unknown location. Then, let M be the number frequency points in the considered frequency range (1–2 GHz). If N such measurements in scanning direction cover the whole pipeline layout, then a reflected signal matrix of $M \times N$ dimension will be formed. In the present case, M is 631 time/frequency points, and N is 20 cross-range points.

(ii) The first reflection (Figure 1) is from the ground surface, which is fixed, and the second and third reflections are from the pipe and crack, respectively.

(iii) Mathematically, the crack detection problem can be modeled in terms of collected real GPR data in N measurements as [14]:

$$y_n(t) = x_n(t) + z_n(t) + s_n(t) \tag{1}$$

where $x_n(t)$ is a reflection from the ground surface, $z_n(t)$ the reflection from the without cracked position of PVC pipe, and $s_n(t)$ the reflection from cracked portions of PVC pipe. To find $s_n(t)$, $x_n(t)$ is known from Figure 2, and researchers have reported various ground reflection methods [7–13] to remove ground reflection $x_n(t)$. In the present case, time gating [15, 16] is used to remove the ground reflection. After removing $x_n(t)$, the resulting data model can be modified as:

$$f_n(t) = z_n(t) + s_n(t) \tag{2}$$

(iv) Figure 2 shows A-scans for non-cracked and cracked PVC pipes In Figure 2, and fixed reflections have been removed by time gating, but non-cracked and cracked PVC pipes show similar responses. Therefore, it is not possible to distinguish whether the PVC pipe is cracked or non-cracked. Similarly, timegated images of non-cracked and cracked PVC pipes are shown in Figure 3. Still, it is difficult to infer from Figure 3(b), which one is the PVC pipe (either cracked or non-cracked).

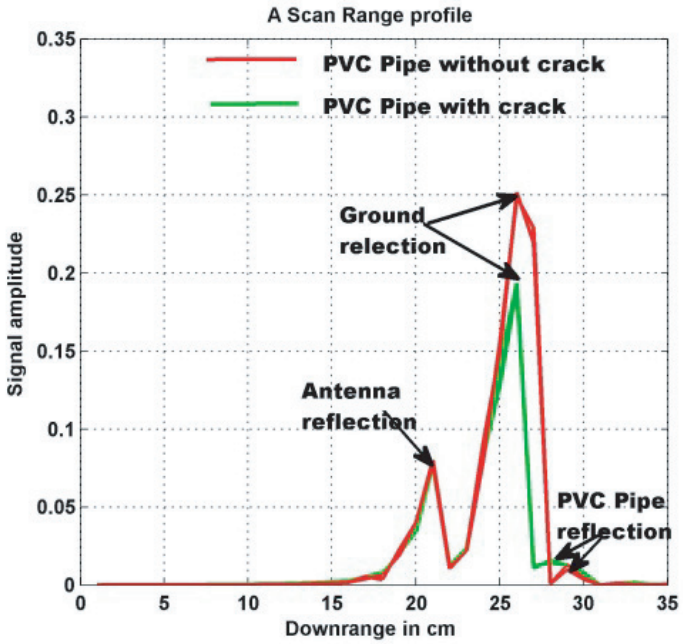

Figure 2. A-scan for (Target-1, Data_{21}) and for (Target-2, Data_{21}).

Therefore, there is a need to develop an algorithm to solve the problem of distinguishing cracked and non-cracked PVC pipes, i.e., a solution of Equation (2) for obtaining $s_n(t)$ which has been discussed in Section 3.

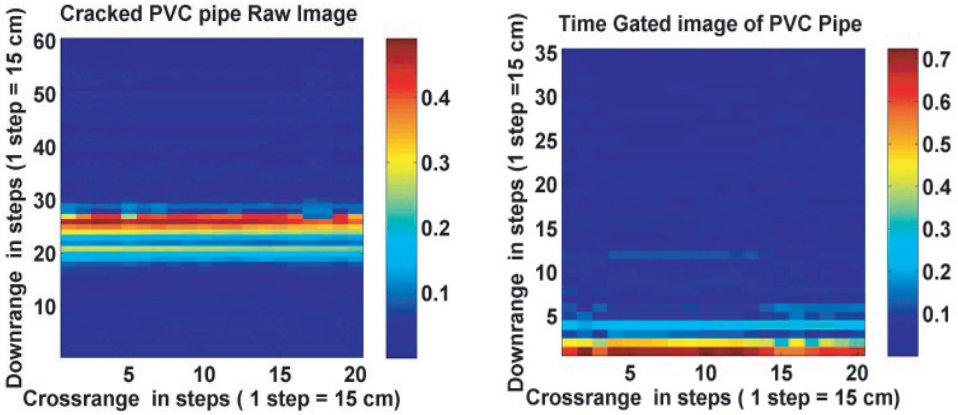

(a) (b)

Figure 3. Effect of time gating. (a) Raw image of PVC Pipe for data id (Target-1, Data_{21}). (b) Time gated image of PVC pipe for data id (Target-1, Data_{21}).

3. ALGORITHM AND IMPLEMENTATION

To solve the crack detection problem, which has been stated in Section 2.1, a novel adaptive algorithm is developed for detecting cracks in a buried PVC pipe. In general, theory of random variables states that if x is a random variable whose mean is μ_x, and variance is σ_x^2, then the random variable, y, defined by $y = ax + b$, where a and b are constants, has mean $\mu_y = a\mu_x + b$ and variance $\sigma_y^2 = a^2\sigma_x^2$. There are many ways to generate the Gaussian distributed random variable such as cumulative distribution function (CDF) inversion method, transformation method, rejection method [21]. However presently, many tools are available to provide an inbuilt random variable generator with a Gaussian distribution, e.g., Matlab has rand$n(m, n)$ utility to generate a random variable with Gaussian distribution. As a large database of ground data is available for various soil moisture contents, it is possible to generate a random variable for a mean and standard deviation of ground data with a Gaussian distribution, which is as follows:

$$f_{Gaussian} = \mu_{gnd} + \sigma_{gnd} X_{gaussian} \tag{3}$$

where $f_{Gaussian}$ is the generated random data for mean of μ_{gnd} and standard deviation of σ_{gnd}, and $X_{gaussian}$ is generated by available Matlab utility. After generating the synthetic data, the overall minimum of covariance matrix of synthetic data (Equation (3)), overall mean of covariance matrix of synthetic data and overall minimum of covariance matrix of GPR data are determined. Normally distributed random data $f_{Gaussian}(t)$ are generated with the same dimensions MxN as real GPR data. The image of synthetic data is shown in Figure 4. Now, covariance matrix of synthetic data serves as a reference for clutter and crack detection, because each cross-range point may have a different covariance due to the variation in the media. Therefore, covariance matrix has dimension NxN. The overall algorithm includes the following steps:

(i) GPR Data are collected along the PVC pipe, presented in Table 1(b). The collected data are of $M \times N$ dimensions, converted from frequency domain to time domain using Inverse Fourier transform. In the present paper, M is 631 which is the number of frequency/time sample points, and N is 20, which is the number of observation/cross-range points for all collected datasets.

(ii) As seen from Figure 3(b), there is a need to verify whether the target is buried, or it is simply ground/clutter, so more processing is required. Therefore, the covariance of timegated data $f_n(t)$ has been adaptively analyzed by the reference covariance of synthetic Gaussian data (Normally distributed). The covariance of timegated data are given by Equation (4):

$$Cov(Timegated) = Cov(f_n(t)) \tag{4}$$

where, covariance of timegated data $Cov(Timegated) = Cov(f_n(t))$ are a matrix of $N \times N$ dimensions. N denotes the number of cross-range points (variable) of GPR measurements.

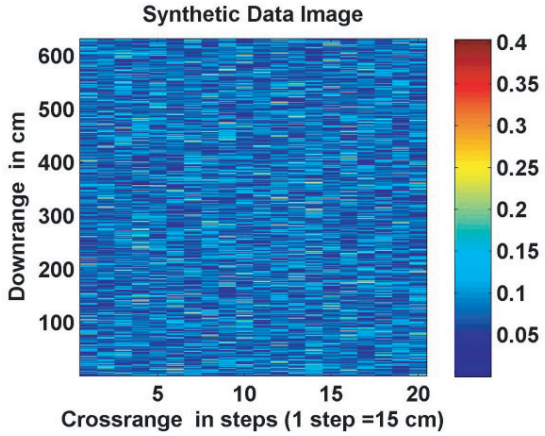

Figure 4. Image of synthetic data.

(iii) The synthetic Gaussian data (Normally distributed) [20] are now taken, with same dimensions $(M \times N)$ as for real GPR data. The covariance of synthetic Gaussian data is given by Equation (5):

$$Cov(SyntheticGaussianData) = Cov(f_{Gaussian}(t)) \tag{5}$$

where covariance of synthetic Gaussian data is a matrix of $N \times N$ dimensions. Real GPR measurements do not follow the Gaussian distribution; therefore, covariance matrix for synthetic data and real GPR data may not have similar statistical characteristics.

(iv) The synthetic data and real GPR do not follow a similar distribution, as the considered synthetic data follow the Gaussian distribution. The real GPR data however may not follow the Gaussian distribution, due to the non-Gaussian process of realtime GPR measurement. Therefore, the minimum covariance of synthetic data is considered as the maximum value of ground/clutter. Hence, to check first whether any target is buried or not, the minimum covariances of synthetic and real GPR data are compared, which is given by Equation (6):

$$CheckT\arg et = \left\{ \begin{array}{ll} \min(cov(timegated)) < \min(cov(synthetic)) & Ground/Clutter \\ Else & Target \end{array} \right\} \tag{6}$$

where *CheckTarget* is the target check to detect the buried target, min*(cover(timegated))* the overall minimum value of covariance matrix of timegated data of real GPR data, and min*(cov(synthetic))* the overall minimum value of synthetic Gaussian data.

(v) Once it is decided that the target is buried, there is a need to check whether the buried target is non-cracked or cracked PVC pipe. Since the mean value of covariance of synthetic data is almost constant, it has been taken as a reference value. If the PVC pipe is non-cracked, then minimum covariance value of a non-cracked pipe is always greater than the minimum value of covariance of a cracked PVC pipe. The minimum value of covariance of timegated data is varied, if the buried PVC pipe is cracked. For this purpose, the minimum value of covariance of timegated real GPR is compared with the mean value of covariance of synthetic Gaussian data, which is given by Equation (7):

$$CheckPVCpipe = \left\{ \begin{array}{ll} \min(cov(timegated)) > mean(cov(synthetic)) & Withoutcracked \\ Else & Cracked \end{array} \right\} \tag{7}$$

where *CheckPVCpipe* is PVC pipe crack and detection check of the buried target; min*(cov(timegated))* is the overall minimum value of covariance matrix of timegated data of real GPR data; *mean(cov(timegated))* is the overall mean value of synthetic Gaussian data.

(vi) After covariance comparison in step (v), the detected non-cracked and cracked PVC pipe features are clearly visualized as shown in Figures 5(a), (b). In Figure 5(a), the maximum intensity represents the detected non-cracked PVC pipe, and in Figure 5(b), the gap between maximum intensities before and after detected cross-range point represents the cracked position of PVC pipe.

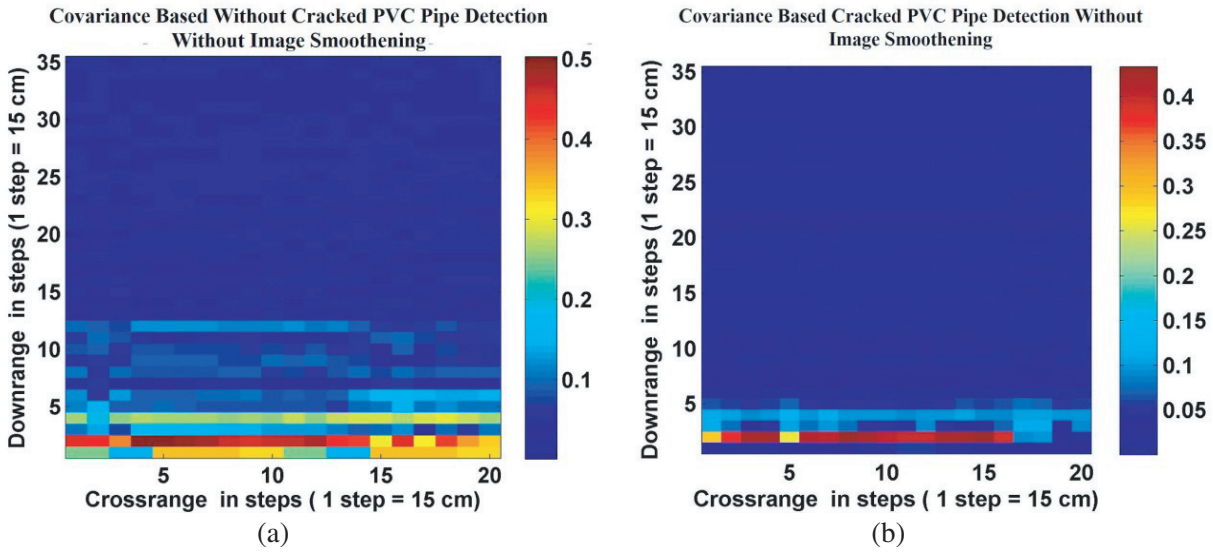

(a) (b)

Figure 5. Covariance based image of PVC pipe. (a) Covariance based image of without cracked PVC pipe. (b) Covariance based image of cracked PVC pipe (crack at 5th step of cross range).

(vii) Image smoothening may help to reduce unwanted effects and equalize the background intensity to enhance the target visualization of covariance based detected images, which are shown in Figures 5(a), (b). The final processed images after image smoothening are shown in Table 2 for non-cracked and cracked PVC pipes. The flowchart for the overall algorithm is shown in Figure 6. Image smoothening is obtained by multiplying the resultant image with the image smoothening factor, which is the minimum value of covariance of synthetic data (step (iv)). The image smoothening factor is as follows:

$$Im_{smoothen} = \min(cov(synthetic)) \tag{8}$$

where min*(cov(synthetic))* denotes the background data (i.e., ground), and $\text{Im}_{smoothen}$ is the image smoothening factor, which is overall minimum of the covariance matrix of synthetic Gaussian data. Thereafter, it is considered as background data in step (iv).
The final processed image is obtained as:

$$\text{Im}_{Final} = \text{Im}_{smoothen} * \text{Im}_{covdetected} \tag{9}$$

where $\text{Im}_{smoothen}$ is the image smoothening factor from Equation (8); $\text{Im}_{covdetected}$ denotes the covariance detected image, which is obtained from step (v); Im_{Final} denotes the final processed images, which is shown in Table 2.

4. RESULT AND DISCUSSION

The developed novel adaptive crack detection algorithm presented in Section 3 is shown in Figure 6. The input real GPR data matrix is of $M \times N$ dimensions, where M represents the number of frequency points at one observation point, and N represents the number of observation points. Similarly, a synthetic Gaussian data (Normally distributed data) matrix of $M \times N$ dimensions is generated (randomly) to compare the covariance of real GPR data with the covariance of synthetic Gaussian data for detecting non-cracked and cracked PVC-pipes, respectively.

The proposed algorithm has been verified experimentally on clutter (i.e., ground), buried non-cracked and buried cracked PVC pipes, and results are shown in Table 2. The considered targets are shown in Table 1(b), and experimentally collected data are denoted by (targets, Dataset$'_i$), where targets are ground, target-1 (without cracked PVC pipe) and target-2 (cracked PVC pipe). The Dataset$'_i$ (where subscript i represents a number of collected data of a target) denote the collected data for corresponding

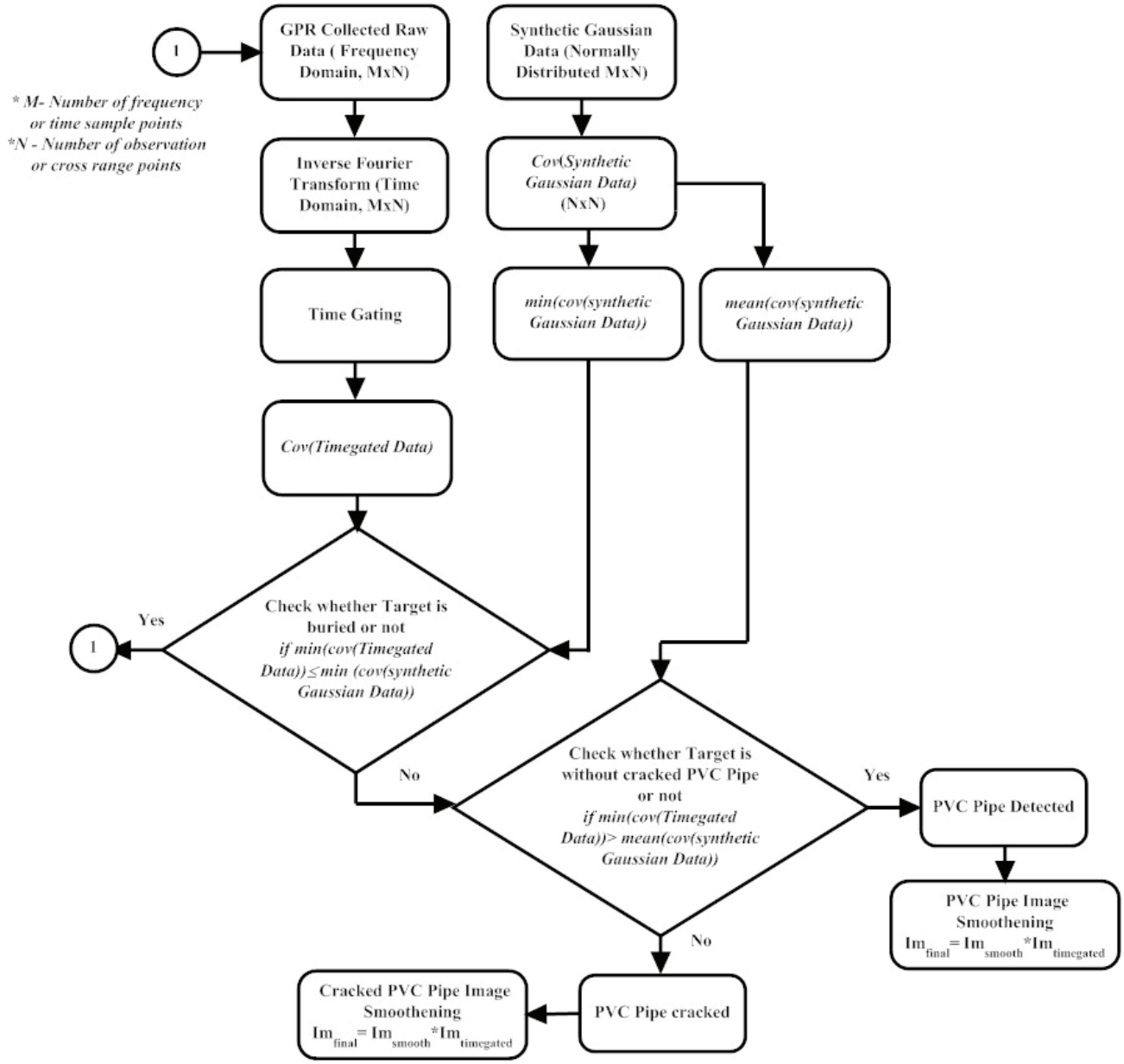

Figure 6. Flow of novel crack detection adaptive algorithm.

depths and moisture level which are shown in Table 1(b). Analyses of resultant images of various buried objects are as the follows:

(i) In Table 2, ground target is considered with ground data id (Ground, GND3), which is shown in Table 1(b). The unprocessed clutter data (i.e., only ground data) have some target like components, denoted by the highest intensity of the unprocessed image in Table 2. After applying the developed algorithm and image smoothening (from Figure 6), a minimum covariance of ground data of 0.000147 and a minimum covariance of synthetic Gaussian data of 0.0000154 are obtained. From step (v) of Section 3 and Equation (6), the minimum covariance of the ground is found greater than the minimum covariance of synthetic Gaussian data; therefore, some underground targets may be buried, and further processing is required. Image of processed ground data with image smoothening is shown in Table 2, where no target is present.

(ii) In Table 2, a non-cracked PVC pipe (i.e., Target-1) is considered as a target with target data

Table 2. Summary of results.

Targets	Covariances	Unprocessed Image	Processed Image by the proposed algorithrm
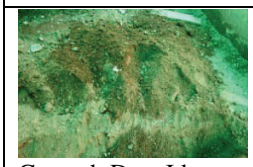 Ground, Data Id: *(Ground,GND_3) from Table 1(b)*	➢ ***Minimum covariance of Ground data =0.000147*** ➢ ***Minimum covariance of synthetic Gaussian Data= 0.0000154***	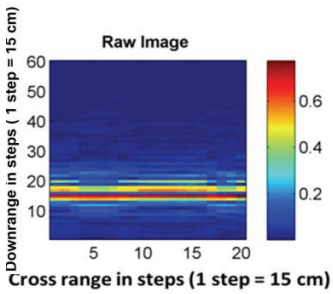	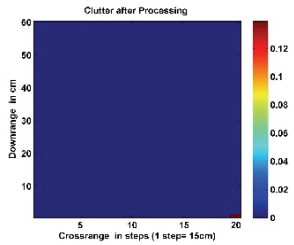
 PVC pipe without crack , Data Id: *(Target-1,$Data_{21}$) from Table 1(b)*	➢ ***Minimum covariance of without cracked PVC pipe= 0.176*** ➢ ***Mean of covariance of synthetic Gaussian Data= 0.0123***	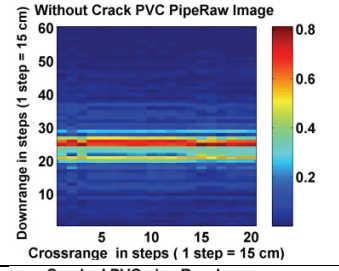	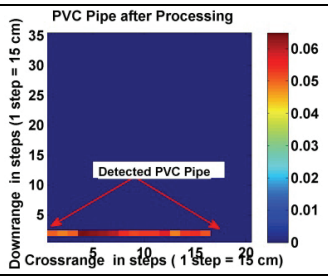
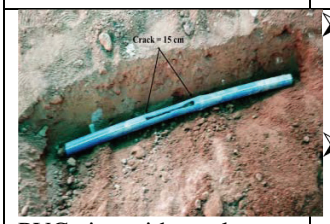 PVC pipe with crack, Data Id: *(Target-2,$Data_{21}$) from Table 1(b)*	➢ ***Minimum covariance of cracked PVC pipe= 0.00956*** ➢ ***Mean of covariance of synthetic Gaussian Data= 0.0123***	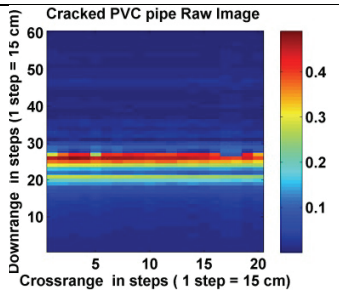	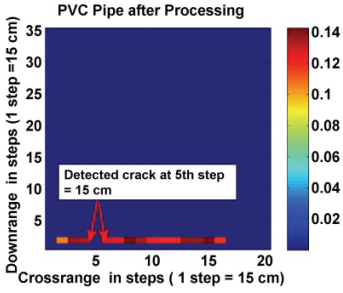

id (target-1, $Data_{21}$), which is shown in Table 1(b). The unprocessed image (Table 2) of PVC pipe data contains target like components and clutter with the same intensity. By applying the developed algorithm and image smoothening (from Figure 6), a minimum covariance of PVC pipe data of 0.0176 and overall mean of covariance of synthetic Gaussian data of 0.0123 are obtained. From step (v) of Section 3 and Equation (7), the minimum covariance of non-cracked PVC pipe is greater than the overall mean of covariance of synthetic Gaussian data; therefore, the buried target is non-cracked PVC pipe, and the processed image after smoothening is shown in Table 2. The non-cracked PVC pipe is clearly visualized.

(iii) In Table 2, the cracked PVC pipe (i.e., Target-2) is considered as a target with target data id (target-2, $Data_{21}$), which is shown in Table 1(b). Same as step (ii) of Section 4, the unprocessed image (Table 2) of cracked PVC pipe data contains target like components and clutter with the same intensity. After applying the developed algorithm and image smoothing (from Figure 6), a minimum covariance of PVC pipe data of 0.00956 and overall mean of covariance of synthetic Gaussian data of 0.0123 are obtained. From step (v) of Section 3 and Equation (7), the minimum covariance of cracked PVC pipe is found less than the overall mean of covariance of synthetic Gaussian data; therefore, the buried target is a cracked PVC pipe. The processed image of the cracked PVC pipe after image smoothening is shown in Table 2, where the cracked PVC pipe is clearly visualized with the cracked location at the 5th cross range step.

To verify the results, data have been collected by changing the cracked location for varying cross-range steps in the cracked PVC pipe. Table 3 shows the results determined with a developed algorithm

Table 3. Covariance data for observations.

Mean of covariance of Synthetic Data	Cracked PVC Pipe		Without cracked PVC pipe	Minimum covariance of synthetic Gaussian (Normal Distributed) Data	Minimum covariance of Ground Data
	PVC-pipe Cracked location	Minimum covariance of cracked PVC Pipe	Minimum covariance of without cracked PVC pipe		
0.0123	5th	0.00951	0.0176	0.0000154	0.000147
0.025	6th	0.0027	0.029	0.0000922	0.000151
0.023	7th	0.00392	0.030	0.0000357	0.000126
0.018	8th	0.0045	0.0193	0.0000147	0.000096
0.028	9th	0.00637	0.037	0.0000532	0.0000089
0.0156	10th	0.00530	0.0332	0.0000469	0.000986
0.0103	11th	0.0051	0.043	0.0003887	0.000729
0.035	12th	0.00326	0.048	0.0000180	0.000146
0.0261	13th	0.00584	0.0341	0.000028	0.00025
0.0197	14th	0.00382	0.0512	0.0000663	0.000493

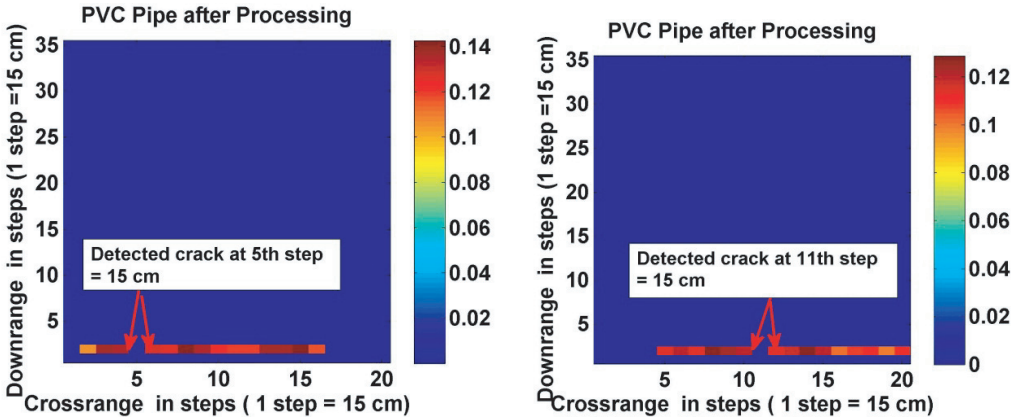

(a) (b)

Figure 7. Validation of developed technique. (a) Image of detected crack at 5th cross-range step. (b) Image of detected crack at 11th cross-range step.

for showing the validity of the algorithm, and the covariance data satisfy Equations (6) and (7). Here, the 5th cross-range step cracked PVC pipe data (i.e., PVC pipe cracked at 5th cross-range step) are taken and processed by the developed technique. The processed image of the 5th cross-range step cracked PVC pipe data is shown in Figure 7(a). The PVC pipe is again changed for observations, in which the cracked location is at the 11th cross-range step. The developed technique (Figure 6) is applied, and the processed image of the 11th cross-range step cracked PVC pipe data is shown in Figure 7(b). In the two cases, the detected crack appears at 5th and 11th cross-range steps in Figures 7(a) and (b), respectively. Hence the developed novel algorithm works effectively for detecting the crack in a buried PVC pipe.

5. CONCLUSION

In this paper, crack detection problem in an underground PVC pipe has been attempted. The results show efficient detection of crack. The covariance of the real GPR data and covariance of normal distributed synthetic Gaussian data are used to detect crack using GPR. During each GPR real-time measurement, the covariance and mean are changed; therefore, selecting the reference for clutter and crack detection is a challenging problem. This problem is solved by generating normally distributed synthetic Gaussian data. Table 2 shows effectiveness of the covariance comparison based adaptive algorithm, where the crack is clearly visualized in the cracked PVC pipe. Figures 7(a), (b) show results of the developed technique. With change in the crack location, the detected crack position is also changed. It may be possible that crack position of a buried PVC pipe is at bottom or side of the PVC pipe, which will limit performance of the developed algorithm. In future, this novel algorithm can be used for commercial underground PVC pipe line crack detection and for underground cable fault detection.

REFERENCES

1. Zhang, H., S. Ouyang, G. Wang, S. Wu, and F. Zhang, "Dielectric spectrum feature vector extraction algorithm of ground penetrating radar signal in frequency bands," *IEEE Geoscience and Remote Sensing Letters*, Vol. 12, 958–962, 2015.
2. Solimene, R., A. Cuccaro, A. Dell'Aversano, I. Catapano, and F. Soldovieri, "Background removal methods in GPR prospecting," *2013 European IEEE Radar Conference (EuRAD)*, 85–88, 2013.
3. Giannakis, I., S. Xu, P. Aubry, A. Yarovoy, and J. Sala, "Signal processing for landmine detection using ground penetrating radar," *IEEE Geoscience and Remote Sensing Symposium (IGARSS)*, 7442–7445, 2016.
4. Solimene, R., A. Cuccaro, A. Dell'Aversano, I. Catapano, and F. Soldovieri, "Ground clutter removal in GPR surveys," *IEEE Journal of Selected Topics in Applied Earth Observations and Remote Sensing*, Vol. 7, 792–798, 2014.
5. Sharma, P., B. Kumar, D. Singh, and S. P. Gaba, "Non-metallic pipe detection using SF-GPR: A new approach using neural network," *IEEE Geoscience and Remote Sensing Symposium (IGARSS)*, 6609–6612, 2016.
6. Sharma, P., S. P. Gaba, and D. Singh, "Study of background subtraction for ground penetrating radar," *IEEE Conferences in Recent Advances in Electronics & Computer Engineering (RAECE)*, 101–105, 2015.
7. Tivive, F. H. C., A. Bouzerdoum, and M. G. Amin, "A subspace projection approach for wall clutter mitigation in through-the-wall radar imaging," *IEEE Transactions on Geoscience and Remote Sensing*, Vol. 53, 2108–2122, 2015.
8. Solimene, R. and A. Cuccaro, "Front wall clutter rejection methods in TWI," *IEEE Geoscience and Remote Sensing Letters*, Vol. 11, 1158–1162, 2014.
9. Zhang, Y., A. S. Venkatachalam, D. Huston, and T. Xia, "Advanced signal processing method for ground penetrating radar feature detection and enhancement," *Proc. SPIE*, Vol. 9063, 906318, 2014.
10. Song, C., Q. Lu, C. Liu, and Y. Gao, "Random noise de-noising and direct wave eliminating in ground penetrating radar signal using SVD method," *IEEE 16th International Conference of Ground Penetrating Radar (GPR)*, 1–5, 2016.
11. Zhang, Y., A. S. Venkatachalam, T. Xia, Y. Xie, and G. Wang, "Data analysis technique to leverage ground penetrating radar ballast inspection performance," *IEEE Radar Conference*, 463–468, 2014.
12. Liu, X., M. Serhir, A. Kameni, M. Lambert, and L. Pichon, "Buried targets detection from synthetic and measured B-scan ground penetrating radar data," *IEEE 11th European Conference on Antennas and Propagation (EUCAP)*, 1726–1730, 2017.
13. Temlioglu, E. and I. Erer, "Clutter removal in ground-penetrating radar images using morphological component analysis," *IEEE Geoscience and Remote Sensing Letters*, Vol. 13, 1802–1806, 2016.

14. Zhang, Y. and X. Tian, "Extracting sparse crack features from correlated background in ground penetrating radar concrete imaging using robust principal component analysis technique," *Nondestructive Characterization and Monitoring of Advanced Materials, Aerospace, and Civil Infrastructure 2016*, Vol. 9804, 2016.
15. Gunatilaka, A. H. and A. B. Brian, "Subspace decomposition technique to improve GPR imaging of antipersonnel mines," *Detection and Remediation Technologies for Mines and Minelike Targets V*, Vol. 4038, 1008–1019, International Society for Optics and Photonics, 2000.
16. Solimene, R., A. D'Alterio, G. Gennarelli, and F. Soldovieri, "Estimation of soil permittivity in presence of antenna-soil interactions," *IEEE Journal of Selected Topics in Applied Earth Observations and Remote Sensing*, Vol. 7, 805–812, 2014.
17. Agarwal, S. and D. Singh, "An adaptive statistical approach for non-destructive underline crack detection of ceramic tiles using millimeter wave imaging radar for industrial application," *IEEE Sensors Journal*, Vol. 15, 7036–7044, 2015.
18. Sharma, P., B. Kumar, D. Singh, and S. P. Gaba, "Critical analysis of background subtraction techniques on real GPR data," *Defence Science Journal*, Vol. 67, 559–571, 2017.
19. David, J. D., *Ground Penetrating Radar*, 2nd Edition, The Institution of Electrical Engineers, London, United Kingdom, 2004, ISBN 978- 86341-360-5.
20. Gao, S., Y. Zhong, and W. Li, "Random weighting method for multisensor data fusion," *IEEE Sensors Journal*, Vol. 11, 1955–1961, 2011.
21. Thomas, D. B., W. Luk, P. H. W. Leong, and J. D. Villasenor, "Gaussian random number generators," *ACM Comput. Surv. 39*, 4, Article 11, October 2007, http://doi.acm.org/10.1145/1287620.1287622